

## Loads Analysis and Structural Optimization of a Long-Range Transport Configuration with Hybrid Laminar Flow Control

Vega Handojo<sup>1</sup>, Thomas Klimmek<sup>2</sup>, Thomas Streit<sup>3</sup>

<sup>1</sup> DLR – Institute of Aeroelasticity, Göttingen, Germany, Vega.Handojo@dlr.de

<sup>2</sup> DLR – Institute of Aeroelasticity, Göttingen, Germany, Thomas.Klimmek@dlr.de

<sup>3</sup> DLR – Institute of Aerodynamics and Flow Technology, Braunschweig, Germany, Th.Streit@dlr.de

### Abstract

This work elaborates the investigation of a long-range transport configuration with hybrid laminar flow control (HLFC) using an iterative pre-design process featuring loads analysis and structural optimization. The HLFC wing was designed with a 3D transonic inverse method. From the loads perspective, the main changes compared to the turbulent counterpart comprise different profile geometries, additional system masses and a backward shift of the front spar to accommodate those additional systems. In the loads analysis, a total of 216 quasi-steady maneuver, 756 dynamic gust cases and one quasi-steady landing case are considered. For the maneuver simulations, a simple maneuver load alleviation (MLA) is implemented. After the post-processing of the loads to extract the sizing relevant ones, a structural optimization is carried out. The constraints in the optimization are maximum strains, 1D buckling and minimum thicknesses. The objective function is the minimization of mass. The cycle comprising loads analysis and structural optimization is conducted iteratively, until the change structural mass – in this case the wing box mass – between two cycles fulfills a defined convergence criterion. Compared to the turbulent counterpart, the HLFC wing box is 0.82% lighter. However, due the additional system masses, the HLFC variant has 0.37% higher operating empty mass, or 0.20% higher maximum take-off mass. Otherwise, the wing load envelopes of HLFC variant are almost identical to those of the turbulent counterpart in general (1.4% more maximum wing root bending moment, 1.1% less maximum root torsion). In the middle wing part, the HLFC aircraft has slightly more nose-down torsion due to the different wing profiles (ca. 6% more minimum torsion and 3% less maximum torsion at 50% span). As a conclusion, the conducted investigation provides an insight into the potential changes in the loads and masses of the HLFC aircraft. On the overall aircraft design level, further studies regarding the changes in the block fuel for a given flight mission or potential changes in the fuel tank layout due to the different wing box geometry can be carried out.

**Keywords:** loads analysis, structural optimization, hybrid laminar flow control, structural mass

### 1. Introduction

The reduction of aircraft fuel consumption has been a crucial research topic in the past years, particularly since it can help to minimize the CO<sub>2</sub> emission of aircraft as well as the airlines' fuel cost. One solution to lower the fuel burn is by reducing the aerodynamic drag. This can be achieved e.g. by delaying the flow transition (from laminar to turbulent) on the aircraft to reduce the friction drag, which makes up a significant fraction of the aerodynamic drag. Known approaches to do so are by designing wings with natural laminar flow (NLF) [1] or hybrid laminar flow control (HLFC) [2]. However, such designs require different wing geometries compared to its turbulent counterpart, so that the flight loads and the dimensions of the primary structure are affected, as the height of the spars and the contour of the skins are different. Both might have an effect on the structural mass. This work focuses on the impact of a HLFC wing design on the flight loads and structural mass of a long-range transport configuration.

## 2. HLFC wing design

The HLFC wing was designed by DLR [2] in the European Union HLFC-WIN project. This design improves the laminar extent of an initial geometry provided by Airbus which is a HLFC variant of the turbulent Airbus research XRF1 geometry. The considered HLFC wing has a different shape between the engine mounting and the wing tip compared to the turbulent counterpart. The laminar boundary layer is restricted to the upper side. For the design, a 3D transonic inverse method was used [3]. A design requirement is to keep the local lift distribution of the Airbus HLFC geometry constant. Otherwise, the wing planform and the profile thicknesses are kept constant. The general trends regarding with the HLFC profiles are that the nose radius is smaller, and the maximum profile thickness is located further downstream. Figure 1 visualizes an exemplary distribution of the skin friction coefficient on the upper side of the HLFC wing, and the transition line is drawn in white. It is apparent that between the engine mounting and the wing tip (where the profile geometries are modified and boundary layer suction is applied), the laminar extent is improved and the skin friction is reduced significantly.

On the aeroelastic side, the different profile shapes are expected to have an influence on the wing stiffnesses, so that changes in the flight loads and thus in the structural mass are possible. In this work, the aircraft with the HLFC profiles is denoted as “HLFC variant”, while the aircraft with the initial profiles is called “turbulent variant”.

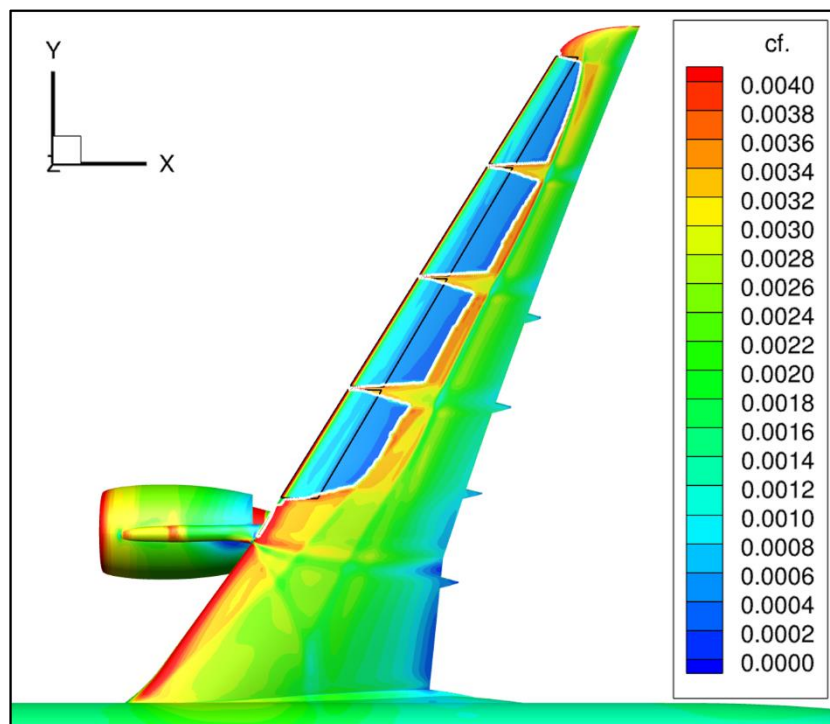


Figure 1 - Exemplary visualization of skin friction coefficient on a HLFC wing

## 3. Reference aircraft and simulation models

The reference aircraft investigated in this work is a composite long-range transport configuration based on the XRF1-DLR-C by Bramsiepe et al. [4], that in turn is based on the Airbus XRF1 (eXternal Research Forum) with a few modifications. The models of the XRF1-DLR-C (both the HLFC and turbulent variant) consist of structural, aerodynamic and optimization models and are generated with the DLR in-house program ModGen [5]. Compared to 2018 [4], changes in the modeling of the aircraft comprise composite stringers and stiffeners, a finer aerodynamic grid and spoiler modeling, as well as the four-split aileron. The latter is intended to serve as a testbed for more comprehensive load alleviation algorithms in future projects. The total area of the ailerons remains the same, and each aileron has the same span.

### 3.1 Structural model

The structure of the lifting surfaces is modelled with shell elements and the fuselage is represented by beam elements. Furthermore, FE models of the control surfaces are added and connected to the main lifting surface box using massless bar elements. Figure 2 visualizes the FE model of the XRF1-DLR-C; the shell elements on the engine nacelles are for illustrational purpose only.

The total mass of the aircraft model comprises structural masses, secondary masses, fuel according to Klimmek [6] and payload. The structural masses result from the material's mass density of the respective shell and bar elements, whereas the remaining masses are modeled with discrete point masses with the respective rotational inertia. For the loads analysis, the global stiffness and mass properties of the FE model are condensed onto the load reference axis (LRA) nodes.

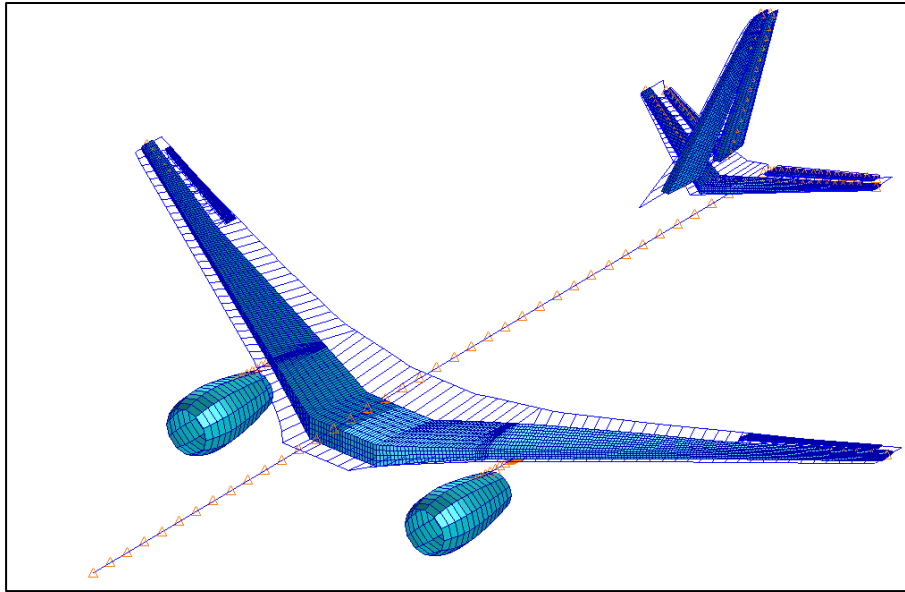


Figure 2 - FE model of the XRF1-DLR-C

### 3.2 Aerodynamic model

The aerodynamic forces are modelled using the doublet lattice method (DLM) [7] which is based on the potential theory. In addition, a slender body element and a corresponding set of interfering lifting surfaces are created to consider the aerodynamic effect of the fuselage [8]. For the lifting surfaces, a twist and camber correction is taken into account, so that the lift at zero angle of attack and the influence of the pitching moment of the HLFC profiles are considered.

For the spoiler aerodynamics, a simplified 2D correction based on the approach used by Binder [9] is implemented, see Figure 3 (LE stands for leading edge, TE stands for trailing edge). To model a 1 deg spoiler deflection, the aerodynamic boxes in front of the spoiler are rotated by -0.05 deg, the deflection of the boxes on the spoiler itself is scaled by 1.1, and the boxes behind the spoiler are rotated by 0.5 deg. Even though the correction might not be accurate to the last percent yet, at least the rotation of the boxes behind the spoiler is included. Because if the boxes behind the deflected spoiler remain unrotated, they would create much lift force which in turn cause a huge amount of nose-down torsion, which is seen as unrealistic. Otherwise, the aerodynamic effectiveness values of all other control surfaces are set to 1.0.

Figure 4 visualizes the aerodynamic model of the XRF1-DLR-C including the slender body for its fuselage. In total, the aerodynamic model comprises approx. 2600 elements.

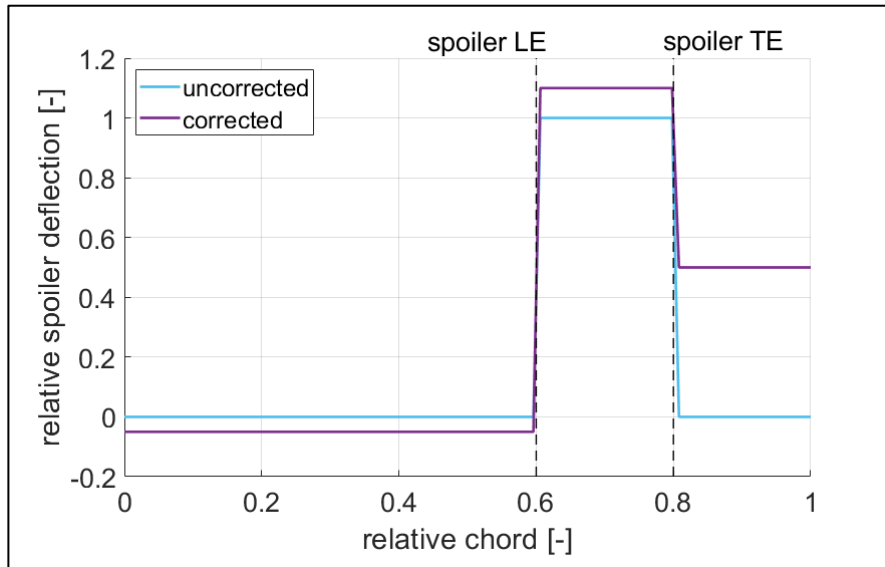


Figure 3 - Illustration of the chordwise correction of spoiler deflection

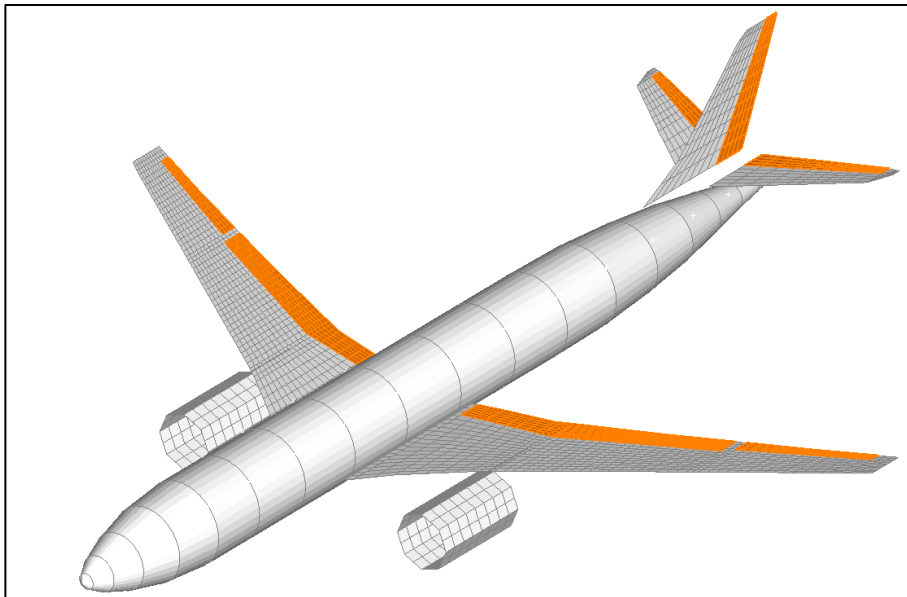


Figure 4 - Aerodynamic model of the XRF1-DLR-C

### 3.3 Changes on the models of the HLFC variant

On the simulation models of the HLFC variant, following changes are made:

- On the FE model, the wing box – particularly the coordinates of the grids of the skins – is adjusted to the HLFC profile geometry. In doing so, the model discretization is kept constant, so that among others the optimization algorithm for the turbulent variant can be taken.
- The position of the front spar is shifted backwards to accommodate the HLFC systems in the profile nose between the engine mounting and the wing tip, see Figure 5. The front spar at the wing tip is located at 33% chord (on the turbulent variant, it lies at 25% chord). Around the engine mounting, the front spar lies at 20% chord (turbulent variant: 15%). At the root, both variants share the same front spar relative position.

Remark: with the backward shift of the front spar, the fuel tank capacities on the HLFC variant would decrease – if the tank layout stayed the same. To have the same fuel masses as on the turbulent variant, the fuel tank layout of the HLFC variant might have to be rethought. To avoid such a big design reconsideration for the fuel mass modeling, and for a better comparability, the fuel masses and their distributions in both variants are assumed to remain the same.

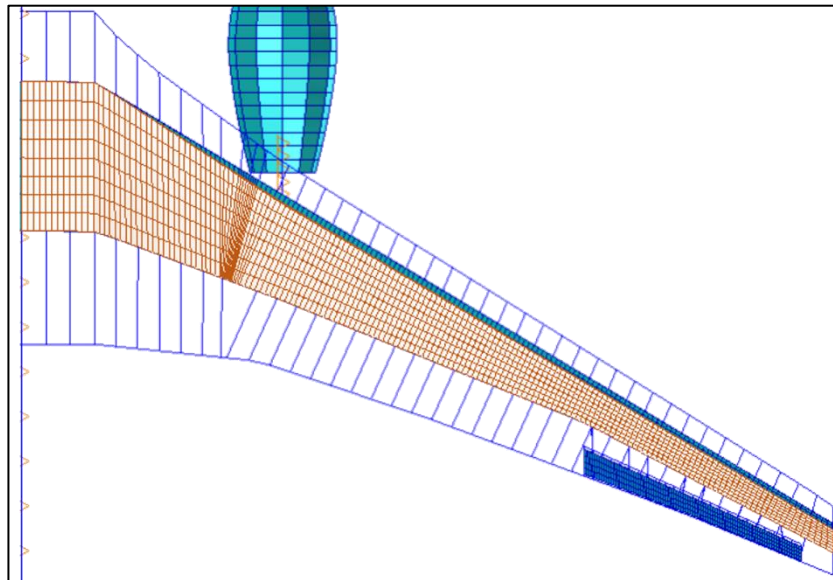


Figure 5 - Comparison of the FE wing box planform between the turbulent variant (cyan, in the background) and the HLFC variant (orange, in the foreground)

- Additional system masses for the HLFC variant are considered. These comprise:
  - Additional perforated titanium skin for the leading edge. With a wetted area of 26 m<sup>2</sup> per wing half, a thickness of 0.8 mm and a mass density of 4500 kg/m<sup>3</sup>, the estimated titanium skin mass per wing half is 93.6 kg.
  - Compressor masses including their mountings and interfaces of 140 kg per wing half.
  - Replacement of slats with Krüger flaps. According to Torenbeek [10], the specific mass of slats for the XRF1 is estimated at 21.96 kg/m<sup>2</sup>, while the specific weight of Krüger flaps is estimated at 22.43 kg/m<sup>2</sup>. With a projected area of approx. 13 m<sup>2</sup> per wing half, a difference of approx. 6 kg results. Furthermore, since Krüger flaps has a smaller maximum span, it is assumed that a total of eight Krüger flaps are necessary to cover the leading edge between the engine mounting and the wing tip which is previously covered by six slats. With the assumption that each Krüger flap and slat has two tracks, the amount of necessary flap tracks increases from 12 to 16. With one slat track weighing 10 kg and one Krüger flap track weighing 12 kg, the mass difference due to the flap tracks is  $16 \cdot 12 \text{ kg} - 12 \cdot 10 \text{ kg} = 72 \text{ kg}$  per wing half. In total, the mass penalty due to the replacement of slats with Krüger flaps is  $6 \text{ kg} + 72 \text{ kg} = 78 \text{ kg}$  per wing half.

The sum of the additional system masses on the HLFC variant is then  $93.6 \text{ kg} + 140 \text{ kg} + 78 \text{ kg} = 311.6 \text{ kg}$  per wing half, or 623.3 kg for the whole span.

- The twist distribution of the HLFC variant is adjusted manually (on the structural and aerodynamic model) so that the spanwise lift distribution during cruise flight has a good agreement (difference of <1.0% in general) with that of the turbulent variant. Figure 6 shows the influence of the modified twist distribution on the local lift coefficient of the elastic aircraft. By only exchanging the profiles, a deficit of 3% at around  $y=23 \text{ m}$  and a surplus of more than 20% are found, compared to the turbulent variant. With an adjustment of the twist distribution, a shift of the spar positions (as mentioned above) and a subsequent structural optimization, the differences can be reduced to below 1% in general, while the surplus at the wing tip is mitigated to around 5%. With one more loop of twist adjustment and subsequent structural optimization, the differences could indeed be reduced to below 0.2%. However, differences of below 1% in the local lift coefficient in general are seen as acceptable.

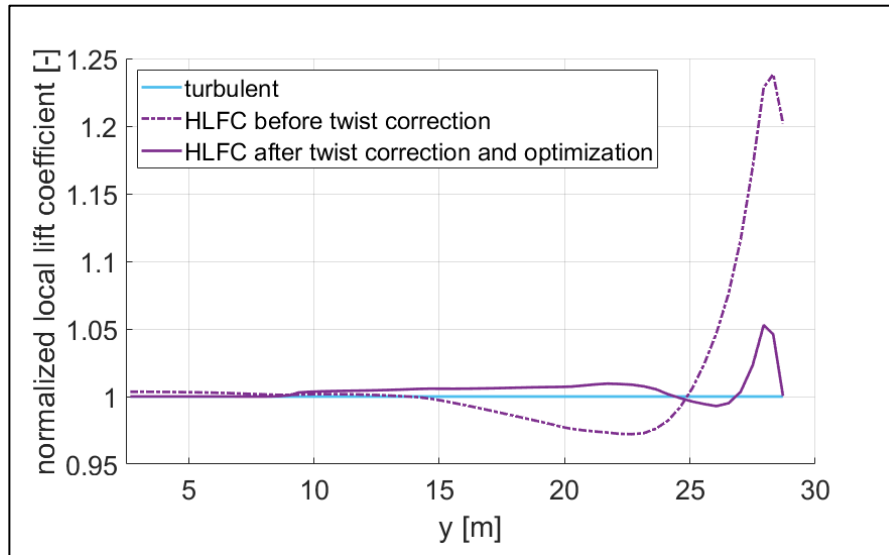


Figure 6 - Influence of twist adjustment on the normalized local lift coefficient

## 4. Methodology

To investigate the loads and the structural mass, both the HLFC and turbulent variant are optimized using an iterative pre-design process based on the MONA process [5]. Each iteration cycle of the process mainly comprises a loads analysis based on the DLR loads process described by Krüger et al. [11] and a subsequent structural optimization with gradient-based algorithms. The Subsections 4.1 to 4.4 describe the main elements and features of the pre-design process briefly, while Subsection 4.5 shows an overview of the workflow.

### 4.1 Loads analysis

In the loads analysis, a total of 216 quasi-steady maneuver cases, 756 dynamic gust cases as well as one quasi-steady landing case are simulated using MSC.Nastran. The relatively large number of load cases is in-line with the requirements of certification specifications (e.g. CS25 [12]). Furthermore, the former is seen as necessary to gain a broader overview of the loads, since a load reduction in one case due to a change in the aircraft stiffness might come together with a load increase in another case, so that the overall load envelope does not necessarily decrease.

The maneuver cases comprise pull-ups, push-downs, accelerated rolls, accelerated yaws as well as accelerated pitch-ups. For the dynamic gust simulations, gust gradients between 9 and 107 m are taken into account. Furthermore, gust cases with airbrake-in and airbrake-out configurations, and two gust directions (upward and downward) are considered.

Table 1 shows an overview of the simulated maneuver and gust load cases. VA stands for the design maneuvering speed, VC for the design cruise speed and VD for the design dive speed. For the ground load case, a simplified 1.5g quasi-steady landing case is taken into account since it has a large contribution in the torsion moment between the wing root and the landing gear mounting.

Since gust simulations output a few hundred time steps for every case, the number of load cases for the structural optimization – with all maneuvers and all time steps of every gust case – would be too high if they were not filtered beforehand. Thus, to limit the number of load cases considered in the structural optimization and with it the size of the optimization task, a loads post-processing with cut load envelopes as used by Handojo [13] is carried out beforehand to extract the relevant load cases. With the loads post-processing, the number of load cases considered in the structural optimization can be reduced to below 100.

Table 1 - Overview of the maneuver and gust load cases.

Load condition	Maneuver	Gust
Mass configurations	<b>9</b> (OEM to MTOM, with center of gravity positions between 18% and 40% of mean aerodynamic chord)	<b>9</b>
Altitudes	<b>3</b> (0 m to 8300 m) The latter is where VC coincides with MC (design cruise Mach number)	<b>3</b>
Maneuvers per altitude	<b>8</b> , comprising: <ul style="list-style-type: none"> <li>• 2.5g pull-ups at VA and VD</li> <li>• -1.0g push-downs at VA and VC</li> <li>• accelerated rolls at VA (0.0 g and 1.67 g)</li> <li>• accelerated yaw at VA</li> <li>• accelerated pitch-up at VA</li> </ul>	
Gusts per altitude		<b>28</b> , comprising: <ul style="list-style-type: none"> <li>• 7 gust gradients (9-107 m) at VC</li> <li>• 2 configurations (airbrake-in and airbrake-out)</li> <li>• 2 gust directions (upward and downward)</li> </ul>
<b>Total</b>	<b>9*3*8 = 216</b>	<b>9*3*28 = 756</b>

#### 4.2 Load alleviation

In the investigated variants of the HLFC and turbulent aircraft, a simple maneuver load alleviation (MLA) algorithm is implemented: During 2.5g pull-ups, all ailerons as well as the three outer spoilers are deflected by  $-20^\circ$  (trailing edge up) in the speed range between the VA and VC. Above VC, the MLA deflection  $\xi_{MLA}$  is assumed to be inversely proportional to the dynamic pressure  $\bar{q}$ :

$$\xi_{MLA}(\bar{q}) = \xi_{MLA}(\bar{q}_C) \frac{\bar{q}_C}{\bar{q}} \Big|_{\bar{q} > \bar{q}_C} \quad (1)$$

Furthermore, it is assumed that the MLA is only activated when the commanded load factor is larger than 1.67g. Hence, during the roll maneuvers at 1.67g, no control surface deflection due to MLA has to be considered.

#### 4.3 Structural optimization

Subsequent to the loads analysis featuring the MLA, a structural optimization is carried out using MSC.Nastran. The objective function is the minimization of mass. The considered constraints are maximum strains, composite plate buckling based on Tetlow [14] – see Equation (2) – and minimum thicknesses.

$$\sigma_{bcT} = \frac{\pi}{6\lambda} \left( \sqrt{E_{11}E_{22}} + \frac{1}{2}v_{12}E_{22} + \frac{1}{2}v_{21}E_{11} + 2\lambda G_{12} \right) \left( \frac{t}{b} \right)^2, \quad (2)$$

with

$$\lambda = 1 - v_{12}v_{21}, \quad (3)$$

and compression buckling stress  $\sigma_{bcT}$  in Pa, longitudinal tensile modulus  $E_{11}$  in Pa, lateral tensile modulus  $E_{22}$  in Pa, Poisson ratios  $v_{12}$ ,  $v_{21}$ , shear modulus  $G_{12}$  in Pa, material thickness  $t$  in m, and buckling field width  $b$  in m. In this case, the buckling field width is set to 0.25 m which approximately represents the gap between stringers on the wing skins.

In the optimization, the laminate parameters, ergo the ply angle distributions, of the skins, spars and ribs are kept constant, so that the design variables are limited to the material thicknesses only. Figure 3 shows the layout of the design fields for the optimization of the wing box which make up a total of 82 design fields – the same spanwise grouping also applies to the spars and ribs.

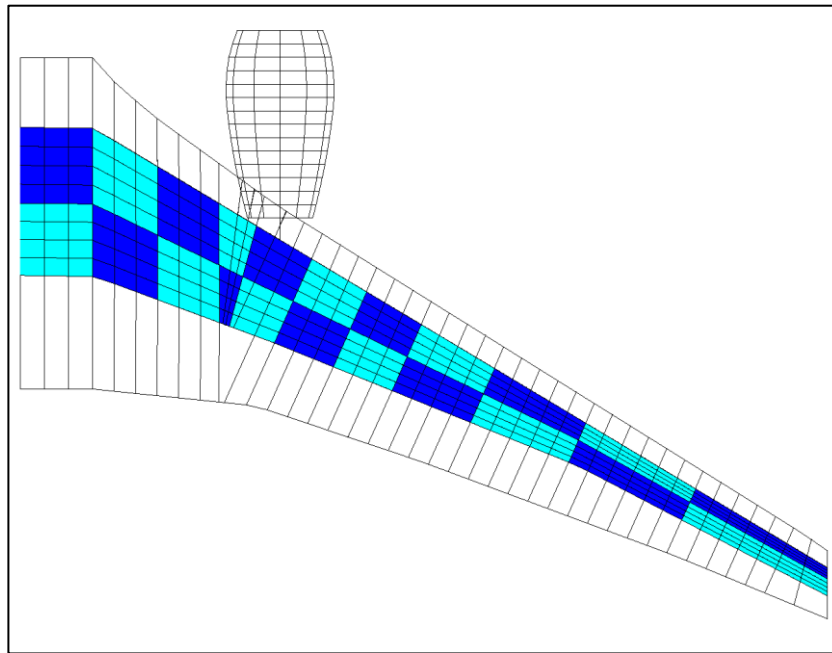


Figure 7 - Design field layout on the wing box

#### 4.4 Aeroelastic checks

After the cycles with the loads analysis and structural optimization reach an adequate mass convergence, a check for the aileron effectiveness of the elastic aircraft as well as a subsonic flutter check is carried out to assess the plausibility of the resulting design. The aileron effectiveness is defined as the ratio of the roll moment derivative due to an aileron deflection between the elastic and rigid aircraft  $\frac{c_{l\xi}(\text{elastic})}{c_{l\xi}(\text{rigid})}$ . The subsonic flutter check is carried out with the KE-method using MSC.Nastran. Both checks are conducted with a reference flight condition of VD+15% at sea level, which corresponds to a Mach number of 0.635 and an equivalent airspeed of 215.9 m/s. Such calculations at sea level brings the advantage that high dynamic pressures – which are an important parameter for aerolastic phenomena such as aileron reversal and flutter – can be reached while staying in the subsonic regime, so that calculations with potential theory aerodynamics are reliable.

#### 4.5 Workflow of the design process

The working steps including the loads analysis and structural optimization are automated in an iterative pre-design process shown in Figure 8. From an initial design, a model condensation is conducted. With the condensed model and the aerodynamic model, gust as well as maneuver simulations are conducted. Since the gust simulations are carried out in the frequency domain and yield only incremental loads, they are superposed with the corresponding 1g trim loads to obtain the total loads acting on the aircraft. Subsequently, the landing loads are calculated, and all resulting loads are post-processed to obtain the sizing relevant ones. With the post-processed loads, a structural optimization is carried out. The cycles of loads analysis and structural optimization are run until a sufficient convergence is reached, in this case a maximum mass change of the wing box of under 0.2% between two cycles. With the converged design, a subsonic flutter check as well as an aileron effectiveness check are conducted.

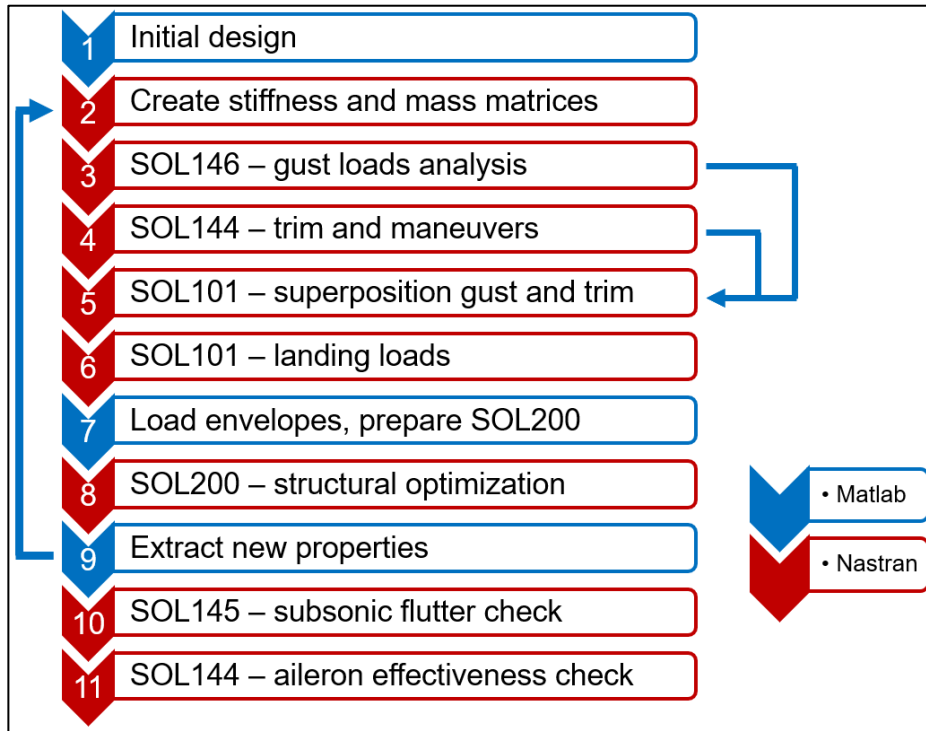


Figure 8 - Workflow of the design process

## 5. Results

This section covers the optimization results of the turbulent and HLFC variant, comprising their load envelopes, their structural properties and selected aeroelastic parameters.

### 5.1 Wing load envelopes

The load envelopes shown in this subsection are calculated in the local coordinate system of the wing, see Figure 9.

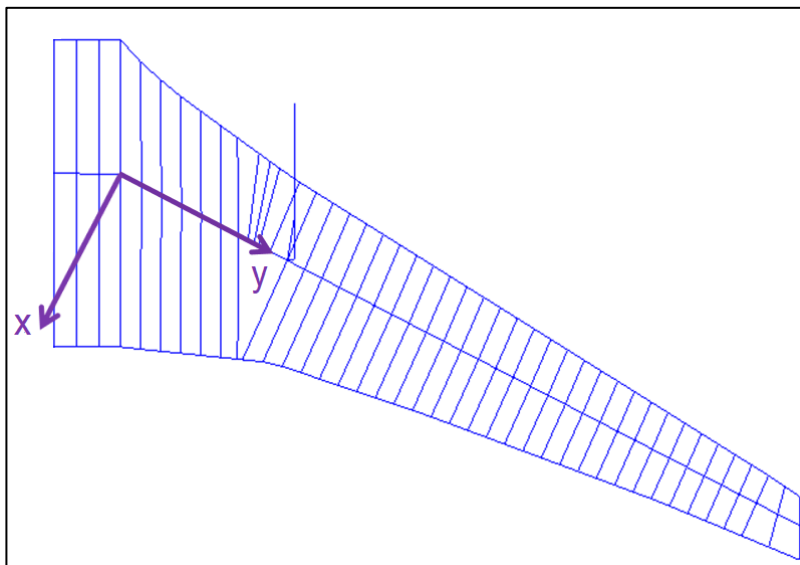


Figure 9 - Local coordinate system for the load evaluation on the starboard wing

Figure 10 shows the resulting wing bending moment ( $M_x$ ) envelopes of the turbulent and HLFC variant. The HLFC aircraft has a slightly larger envelope with 1.4% higher maximum bending moment at the wing root. For the envelope of negative bending moment, the HLFC variant shows a magnitude that is 4.1% larger compared to the turbulent counterpart. Furthermore, the maximum bending moments are mainly reached in gust encounters, while the minimum values are generally reached during maneuvers.

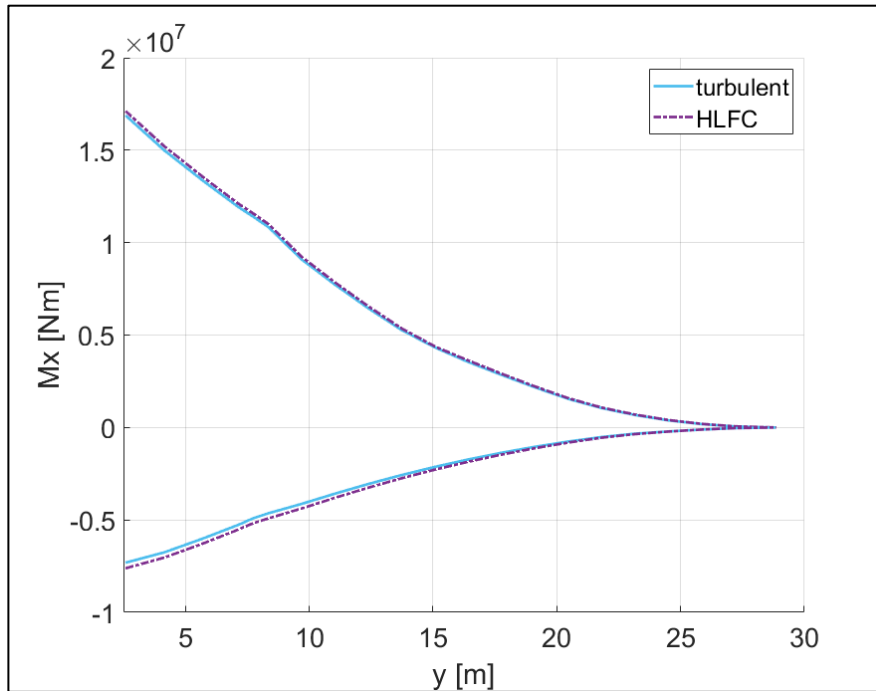


Figure 10 - Comparison of the wing bending moment envelopes

In the torsion moment ( $M_y$ ) envelope shown in Figure 11, the HLFC generally shows a slight shift towards negative torsion (ca. 6% more minimum torsion and 3% less maximum torsion at 50% span) which is caused by the different profiles. At the wing root, the HLFC variant has 1.1% less maximum torsion moment. Outboard of the engine (ca.  $y > 9$  m), the maximum torsion moments are reached during maneuvers. Between the root and the engine (ca.  $2.5 \text{ m} < y < 9 \text{ m}$ ), gust cases are found in the maximum torsions. The minimum torsions are reached during maneuvers (outboard of the landing gear, ca.  $y > 7$  m) and during the landing impact (between the root and the landing gear, ca.  $2.5 \text{ m} < y < 7 \text{ m}$ ).

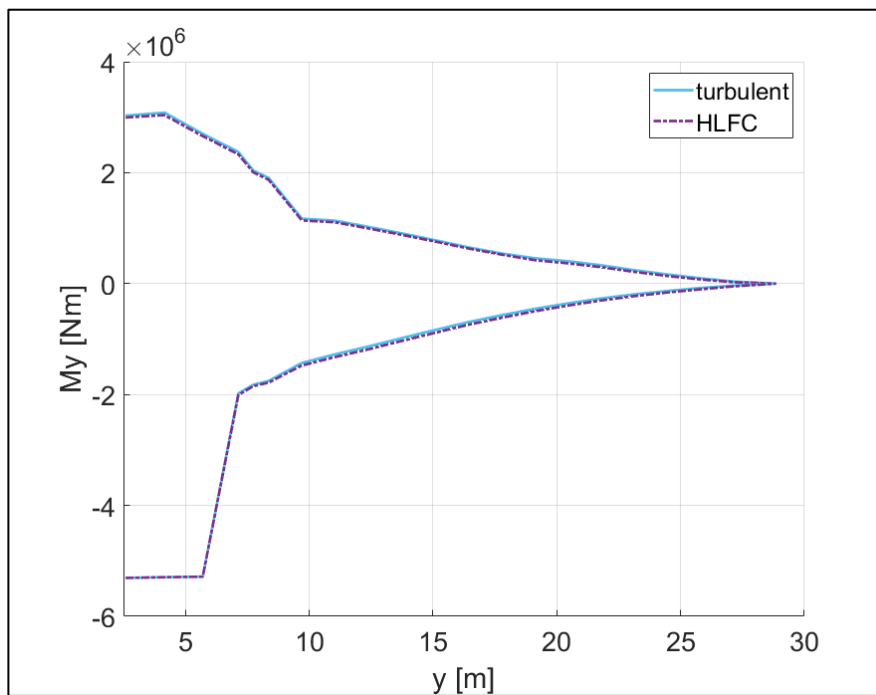


Figure 11 - Comparison of the torsion moment envelopes on the wing

## 5.2 Structural properties

Figure 12 and Figure 13 show the thickness distribution of the wing box of the turbulent variant and the HLFC variant, respectively. The most striking difference is that around the middle part of the wing, the HLFC variant has higher thickness values at the front half of the skins. Otherwise, the general trends on both wing boxes are similar: the highest skin thicknesses are found near the engine position, the upper skin is in general thicker than the lower skin, the spar and ribs are close to the minimum thickness of 4 mm except near the engine and landing gear mounting.

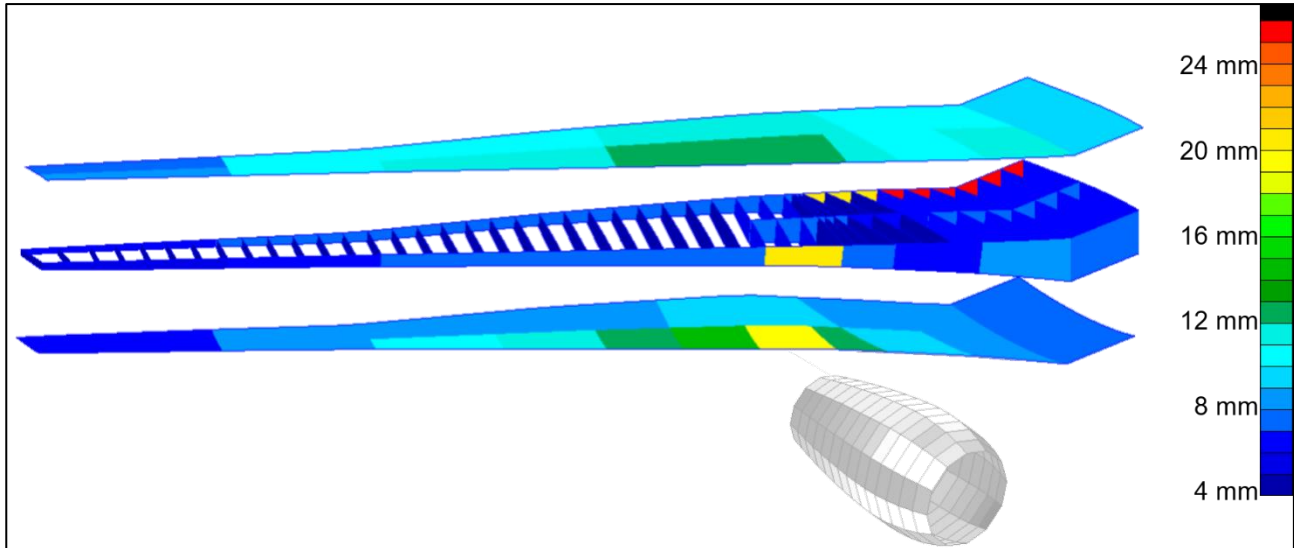


Figure 12 - Wing material thicknesses on the turbulent variant

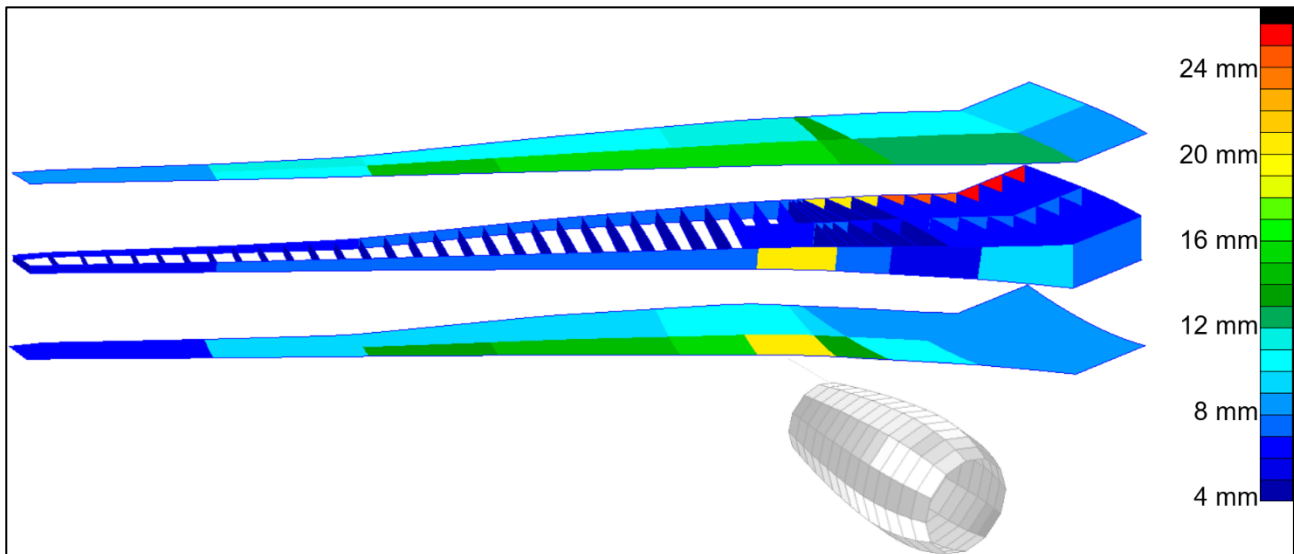


Figure 13 - Wing material thicknesses on the HLFC variant

Despite the higher thicknesses on the front half of the skin, the wing box of the HLFC variant is around 112.6 kg or lighter compared to that of the turbulent variant, see Table 2. The lighter mass is explained through the lower chord of the HLFC wing box, which results in smaller surface areas of the skins and ribs. The mass reduction through the smaller skin and rib areas outweighs the mass increase due to the higher thicknesses of the skins.

Table 2 - Comparison of wing box component masses, tip to tip

Wing box component	Turbulent	HLFC
Upper skin	2931.8 kg	2890.8 kg
Upper stringers	1229.8 kg	1238.0 kg
Lower skin	2613.4 kg	2588.8 kg
Lower stringers	1103.4 kg	1109.8 kg
Ribs and spars	3468.2 kg	3417.3 kg
Rib and spar stiffeners	2038.8 kg	2028.2 kg
<b>Total wing box mass</b>	<b>13385.4 kg</b>	<b>13272.8 kg</b>

However, if the comparison is done with the operating empty mass, the HLFC variant is around 480 kg heavier, see Table 3. With an empty operating mass of around 130 tons, the HLFC variant is around 0.37% heavier. The mass increase is caused by the additional system masses on the HLFC aircraft, despite the lower structural masses on the wing box and HTP box. Remark: the mass summation is carried out with the assumption that the primary structures represent ideal load-carrying structures (no mass penalties due to joints, fasteners, access holes and local reinforcements). If those mass penalties should be considered, an empirical mass factor as proposed by Chiozzotto [15] can be applied to the primary structures, in this case to the wing box, HTP box and VTP box. The same mass factor can also be applied to the mass differences of those primary structures.

Table 3 - Component mass differences between the turbulent and HLFC variant

Aircraft component/assembly	Mass difference HLFC-turbulent
Wing box, tip to tip	-113 kg
Additional HLFC systems, tip to tip	623 kg
HTP box, tip to tip	-31 kg
VTP box	+0 kg
<b>Whole aircraft (operating empty mass)</b>	<b>+480 kg</b>

In addition, the first symmetric wing bending frequency of the HLFC variant at the operating empty mass is 0.83% smaller compared to the turbulent counterpart, which is assumed to be partly caused by the additional system masses.

### 5.3 Aeroelastic parameters

The investigated aeroelastic parameters comprise the aileron effectiveness and the first flutter speed which are calculated in the subsonic regime (see Subsection 4.4).

As mentioned in Section 3, the reference aircraft has four ailerons on each side of the wing, and its layout is shown in Figure 14. Table 4 lists the values of the aileron effectiveness for all four ailerons. It is apparent that up to  $VD+15\%$ , neither of the variants shows any aileron reversal, and the aileron effectiveness values are comparable between both variants. Nevertheless, aileron 3 and 4 of the HLFC variant are slightly less effective, whereas aileron 1 is as effective as on the turbulent variant.

For the flight mechanics, those differences are marginal. From the aeroelastic perspective however, the lower effectiveness of aileron 3 and 4 of the HLFC variant is seen to be caused by the backward shift of the front spar. That backward shift of the spar decreases the wing box chord and thus the torsional second moment of area, which cannot fully be compensated by increasing the skin thicknesses. As a result, the wing box of the HLFC variant has a slightly lower torsional stiffness. This effect of lower torsional stiffness is more visible toward the wing tip, which is indicated by the aileron effectiveness values dropping faster (from aileron 1 to aileron 4) compared to the turbulent variant.

Regarding the flutter speed, the HLFC variant shows a slightly lower flutter speed compared to the turbulent variant, see Table 4. According to the subsonic flutter calculation using the KE-method, both variants do not flutter up to airspeeds of  $VD+15\%$  at sea level.

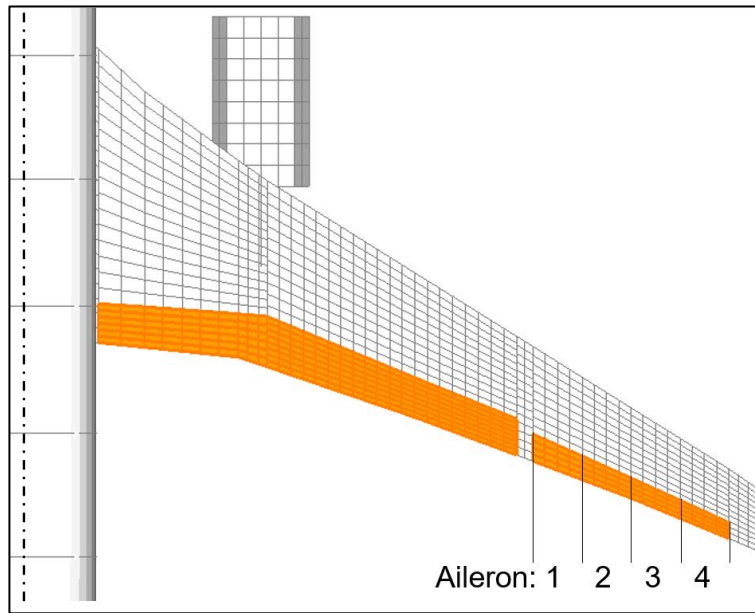


Figure 14 - Visualization of the aileron layout

Table 4 - Comparison of the aeroelastic parameters

Aeroelastic parameter		Turbulent	HLFC
Aileron effectiveness	Aileron 1	0.420	0.421
	Aileron 2	0.306	0.304
	Aileron 3	0.192	0.181
	Aileron 4	0.063	0.037
First flutter speed		303.17 m/s EAS	289.12 m/s EAS

## 6. Conclusions and outlook

An investigation of the HLFC variant of a long-range transport aircraft using an iterative design process featuring loads analysis and structural optimization has been carried out. The comparisons with its turbulent counterpart comprise the resulting load envelopes, structural properties and masses, as well as aeroelastic properties.

Regarding the loads, both variants only differ slightly, with the HLFC variant having 1.4% higher maximum wing root bending moment and 1.1% lower maximum wing root torsion. Furthermore, the HLFC variant generally shows a slight shift in the torsion moment towards the negative direction (nose-down torsion) due to the different profiles.

In the front half, the HLFC wing box has higher skin thicknesses. Nevertheless, the whole wing box is 112.6 kg lighter compared to the turbulent counterpart due to the backward shift of the HLFC front spar, which decreases the areas of the skins and ribs. However, the operating empty mass of the HLFC variant is around 0.37% higher compared to the turbulent counterpart due to the additional system masses. If referred to the maximum take-off mass, the HLFC variant is 0.20% heavier.

Up to airspeeds of  $VD+15\%$  at sea level, neither of the variants shows any aileron reversal, and the values of the aileron effectiveness are comparable between both variants. A subsonic flutter check yields a first flutter speed of the HLFC aircraft that is 4.6% lower than the turbulent counterpart. Nevertheless, the first flutter speeds on both configurations are significantly above  $VD+15\%$ .

One aspect that can be investigated in the future is the trade-off between drag reduction (through the HLFC system) and the resulting mass increase of the aircraft. With a given flight mission, the change in the necessary block fuel for the HLFC variant can be estimated.

On the overall aircraft design level, the impact of the backward shift of the front spar on the fuel tank capacity can be investigated. One way to compensate the decreased fuel capacity is to modify the fuel tank layout, e.g. that a fraction of the surge tanks is used as regular tanks. Otherwise, since the majority of long-range transport aircraft are not flown at the maximum range (with the maximum fuel mass), it can be discussed whether a range decrease in the payload-range diagram due to the lower fuel capacity is acceptable or not.

## **7. Acknowledgment**

The authors thank the Federal Ministry for Economic Affairs and Energy (Bundesministerium für Wirtschaft und Energie - BMWi) for the funding as part of LuFo V-3 in the project In-Fly-Tec/APLAUS. Furthermore, the authors thank the colleagues from the Institute of Aerodynamics and Flow Technology for providing visualizations of CFD simulations with the HLFC wing, the HLFC wing box layout and data for HLFC system masses.

## **8. Contact author email address**

The email address of the contact author is: [vega.handojo@dlr.de](mailto:vega.handojo@dlr.de)

## **9. Copyright statement**

The authors confirm that they, and/or their company or organization, hold copyright on all of the original material included in this paper. The authors also confirm that they have obtained permission, from the copyright holder of any third party material included in this paper, to publish it as part of their paper. The authors confirm that they give permission, or have obtained permission from the copyright holder of this paper, for the publication and distribution of this paper as part of the ICAS proceedings or as individual off-prints from the proceedings.

## References

- [1] Seitz, A. und Kruse, M. und Wunderlich, T. und Bold, J. und Heinrich, L., "The DLR Project LamAiR: Design of a NLF Forward Swept Wing for Short and Medium Range Transport Application," 29th AIAA Applied Aerodynamics Conference, 27 – 30 June 2011, Hawaii, USA, 2011.
- [2] Streit, T., Kruse, M., Kilian, T., v. Geyr, H., Petropoulos, I., "Aerodynamical Design and Analysis of HLFC Wings within the European Project HLFC-WIN", 33rd Congress of the International Council of the Aeronautical Sciences, 4-9 September 2022, Stockholm, Sweden., tbp
- [3] Streit, T., Hoffrogge, C., "DLR transonic inverse design code, extensions and modifications to increase versatility and robustness," *The Aeronautical Journal*, 2017, 121, (1245), pp 1733-1757, <https://doi.org/10.1017/aer.2017.101>, 2017.
- [4] Bramsiepe, K., Handojo, V., Meddaikar, Y. M., Schulze, M., and Klimmek, T., "Loads and Structural Optimisation Process for Composite Long Range Transport Aircraft Configuration," AIAA Aviation Forum, Multidisciplinary Analysis and Optimization Conference, Atlanta, Georgia, USA, 2018.
- [5] Klimmek, T., "Parametric Set-Up of a Structural Model for FERMAT Configuration for Aeroelastic and Loads Analysis," *ASD Journal*, vol. 3, no. 2, pp. 31–49, 2014.
- [6] Klimmek, T., "Statische aeroelastische Anforderungen beim multidisziplinären Strukturentwurf von Verkehrsflugzeugflügeln," Doctoral Thesis, Technische Universität Braunschweig, Braunschweig, 2016.
- [7] Albano, E., and Rodden, W., "A Doublet Lattice Method for Calculating Lift Distributions on Oscillating Surfaces in Subsonic Flows," *AIAA Journal*, vol. 7, no. 2, 1968.
- [8] Giesing, J. P., Kálmán, T. P., and Rodden, W. P., "Subsonic Steady and Oscillatory Aerodynamics for Multiple Interfering Wings and Bodies," *Journal of Aircraft*, vol. 9, no. 10, 1972.
- [9] Binder, S., "Simultaneous Optimisation of Composite Wing Structures and Control Systems for Active and Passive Load Alleviation," Doctoral Thesis, Delft University of Technology, Delft, 2021.
- [10] Torenbeek, E., "Development and Applications of a Comprehensive, Design-sensitive Weight Prediction Method for Wing Structures of Transport Category Aircraft", Report LR-693, Delft University of Technology, Delft, 1992.
- [11] Krüger, W., and Klimmek, T., "Definition of a Comprehensive Loads Process in the DLR Project iLOADS," *Deutscher Luft- und Raumfahrtkongress*, 2016.
- [12] European Aviation Safety Agency, CS25 - Certification Specifications and Acceptable Means of Compliance for Large Aeroplanes, Amendment 23, 2019.
- [13] Handojo, V., "Contribution to Load Alleviation in Aircraft Pre-design and Its Influence on Structural Mass and Fatigue". DLR-Forschungsbericht. DLR-FB-2020-47. Doctoral Thesis, Technische Universität Berlin, 2021.
- [14] Tetlow, R., "Design Charts for Carbon Fibre Composites," Technical Report, Cranfield Institute of Technology, Cranfield, 1970.
- [15] Pinho Chiozzotto, G., "Improving Aircraft Conceptual Design with Methods for Wing Loads, Aeroelasticity and Mass Estimation", Doctoral thesis, Technische Universität Berlin, Berlin, 2017